

Article

Adsorption of Methyl Orange on a Novel Palygorskite/UiO-66 Nanocomposite

Ioanna A. Vasiliadou ^{1,*}, Thaleia Ioannidou ¹ , Maria Anagnostopoulou ², Antonios Polyzotou ¹,
Dimitrios Papoulis ³  and Konstantinos C. Christoforidis ^{1,2,*} 

¹ Department of Environmental Engineering, Democritus University of Thrace, 67100 Xanthi, Greece; thaioann@env.duth.gr (T.I.); antopoly3@env.duth.gr (A.P.)

² Institute of Chemistry for Energy, Environment and Health, Centre National de la Recherche Scientifique (CNRS), University of Strasbourg, 25 rue Becquerel, 67087 Strasbourg, France; managnostopoulou@unistra.fr

³ Department of Geology, University of Patras, 26504 Patras, Greece; papoulis@upatras.gr

* Correspondence: ioavasil@env.duth.gr (I.A.V.); kochristo@env.duth.gr (K.C.C.)

Abstract: Herein, a novel composite material containing UiO-66 and palygorskite (Pal) clay mineral was prepared using a facile one-pot synthesis process. The material was studied using a variety of techniques and applied as did not affect the structure of the metal-organic framework (MOF) part, but induced a small increase in specific surface area. The developed Pal/UiO-66 composite presented excellent adsorption efficiency against MO removal, as evidenced by detailed kinetic and isotherm experiments. An impressive maximum adsorption capacity at equilibrium was evidenced; 340 mg g⁻¹ at pH = 5 and T = 25 °C. This corresponds to a 34.5 % increase compared with pure UiO-66, considering only the MOF content. Furthermore, the Pal/UiO-66 composite was proven stable and highly recyclable, losing less than 9% of the removal capacity after five consecutive cycles. The study highlights the synergistic effect of the coupling of MOF structures with low-cost and abundant clay minerals for the development of advanced absorbents.

Keywords: metal–organic frameworks; UiO-66; palygorskite; methyl orange; dye adsorption



Citation: Vasiliadou, I.A.; Ioannidou, T.; Anagnostopoulou, M.; Polyzotou, A.; Papoulis, D.; Christoforidis, K.C. Adsorption of Methyl Orange on a Novel Palygorskite/UiO-66 Nanocomposite. *Appl. Sci.* **2022**, *12*, 7468. <https://doi.org/10.3390/app12157468>

Academic Editor: Chang-Gu Lee

Received: 9 July 2022

Accepted: 21 July 2022

Published: 25 July 2022

Publisher's Note: MDPI stays neutral with regard to jurisdictional claims in published maps and institutional affiliations.



Copyright: © 2022 by the authors. Licensee MDPI, Basel, Switzerland. This article is an open access article distributed under the terms and conditions of the Creative Commons Attribution (CC BY) license (<https://creativecommons.org/licenses/by/4.0/>).

1. Introduction

Natural environments, and especially water bodies, receive high amounts of xenobiotics due to human activities [1]. Synthetic dyes represent a class of organic pollutants that end up in wastewater in high amounts, having detrimental effects on the natural environment [2]. They are commonly used in different production lines such as the paper, printing, textile, food, and pharmaceutical industries. The annual discharge of dyes and wastes containing high amounts of dyes into water streams worldwide by textile industries is estimated to be around 5000–8000 tons [3–5], and many of the dyes found in industrial wastes are harmful for living organisms [6]. Different technologies have been developed and applied for dye removal from effluents, including biological treatment, advanced oxidation, membrane separation, and adsorption [7–9]. However, some of these methods are insufficient, and they may require the use of specialized set-ups or the introduction of chemicals that end up in the environment [10,11]. Among the different processes suggested, adsorption is probably the most effective method for contaminated water treatment for the removal of a variety of pollutants, both organic and inorganic. This is mostly due to operational advantages, simplicity, high efficiency, and cost effectiveness [12–15].

In absorption processes, efficiency is solely defined by the absorbent. Therefore, given their vital role, many different types of adsorbents, such as natural media and bioproducts of another process [16,17], activated carbon [18], and synthetic porous materials [19], have been applied in wastewater treatment. Among the different types of absorbents, natural clay minerals have been identified as decisive media for dye adsorption due to their inherent

properties such as nontoxicity, swelling, cation exchange, significant surface capacity, and their wide availability [20,21]. However, although untreated natural clays have high cation exchange capacity due to their negatively charged layers, they present significant limitations in anion adsorption [22,23]. Palygorskite is characterized by micro-fibrous morphology with a $\text{Si}_8\text{O}_{20}\text{Al}_2\text{Mg}_2(\text{OH})_2(\text{OH}_2)_4 \cdot 4\text{H}_2\text{O}$ structural formula [24]. It possesses excellent physical and chemical properties, showing high potential for industrial, catalytic, and environmental cleaning-up applications [23,25–27]. Usually, chemical or thermal surface modification is a prerequisite to increase the adsorption ability against anionic chemical moieties [28,29]. This adds an extra step to the development of efficient absorbents.

Metal–organic frameworks (MOFs) are a new class of synthetic materials that possess highly crystalline and porous structures. MOFs have been effectively applied as solid absorbing media in the gas and the liquid phases, including dye removal [3,11,30,31]. They are made of metal clusters or metal ions that are connected together with organic linkers, forming a highly porous structure. Different MOF structures have been studied for the removal of organic dyes, such as UiO-66, MIL-family, ZIF-8, and their derivatives [3,11,32]. Due to the vast range of ligands and metal nodes, their properties can be fine-tuned toward a specific application, including dye adsorption [3,33]. Among the different MOF structures, UiO-66 and its derivatives have received great attention due to their great stability and exceptional tunability and functionality [34]. As a general rule, dye adsorption is mostly driven through electrostatic interactions, although other mechanisms may occur, i.e., via π – π interactions [3,11]. Yang showed the great efficiency of UiO-66 and modified versions with immobilized phosphate over a range of dyes including anionic dyes [35]. However, other studies showed low removal efficiency via adsorption of methyl orange (MO) using UiO-66 and its NH_2 – derivative [36]. This highlights the importance of the synthesis conditions used for the development of absorbents. Very recently, Far et al. developed composite absorbents made of monometallic Cr-MOF, bimetallic CoNi-MOF, and clay minerals [37]. A significant improvement in dye adsorption was observed compared with the removal efficiency of the clay.

Herein, palygorskite clay mineral (Pal) of micro-fibrous morphology was coupled with UiO-66 using a facile one-step open-vessel thermal process. The structure, composition, morphology, and the textural properties of the prepared materials were studied using X-ray diffraction (XRD), attenuated total reflectance (ATR), N_2 physisorption, and thermogravimetric analysis (TGA). The results of adsorption experiments revealed that the adsorption efficiency against MO removal of the composite bearing 90 wt.% of UiO-66 was improved by ~21% compared with that of pure UiO-66. This was raised to a ca. 34% improved efficiency taking into account the UiO-66 content. The present study highlights the importance of developing MOF-based composites via coupling with low-cost and abundant materials for the development of advanced absorbents.

2. Materials and Methods

2.1. Materials

All chemicals were purchased from Sigma Aldrich (Germany) and were used as received. The palygorskite (Pal) sample was obtained from the Ventzia continental basin, Western Macedonia, Greece. Gravity sedimentation was used to obtain particles $<2 \mu\text{m}$. The clay fraction was collected by centrifugation [25,26]. Composites were obtained using only the clay fraction. Clay was used without any thermal pretreatment.

2.1.1. Synthesis of UiO-66

A synthesis protocol previously developed was used for the preparation of pure UiO-66 [31,38]. Typically, 1.25 g of ZrCl_4 (Aldrich, 99.5%) was added to 50 mL *N,N*-dimethyl formamide (DMF, 99.9%), followed by the addition of 10 mL acetic acid and sonication for 20 min. A second solution was prepared by adding 1.23 g of terephthalic acid to 100 mL DMF followed by 20 min of sonication. The two solutions were mixed in a round-bottom flask. The solution was heated under stirring to 150 °C for 24 h in an

oil bath. After naturally cooling to room temperature, the material was recovered and washed three times with ethanol and once with acetone using centrifugation. Activation was performed by exchanging the solvent with acetone over a period of four days. The solvent was changed every second day. Finally, the material was dried at 100 °C overnight and stored in a desiccator for further use. The yield of the synthesis was 1.095 g.

2.1.2. Synthesis of Palygorskite/UiO-66 Composite

A similar synthesis process with a slide modification was used for the development of the palygorskite/UiO-66 composite (Pal/UiO-66). First, 0.1 g of Pal was placed in 50 mL of DMF and sonicated for 30 min. Then, 0.83 g of $ZrCl_4$ and 10 mL of acetic acid were added and further sonicated for 20 min. A second solution containing 0.81 g of terephthalic acid and 100 mL DMF was prepared. The two mixtures were placed in a round-bottom flask and then received the same heating treatment as described in the pure UiO-66 protocol. The material was collected, washed, and activated following the same steps as those for the pure UiO-66. The Pal amount used for the development of the composite corresponded to 10 wt.% of Pal with respect to the yield of the pure UiO-66 synthesis. The yield of the synthesis was 0.838 g.

2.2. Materials Characterization

X-ray diffraction (XRD) measurements were performed using a Bruker D8-Advance diffractometer (Karlsruhe, Germany) equipped with a Lynx-Eye detector operating at 40 kV and 40 mA, using $Cu K_{\alpha}$ radiation at 1.5418°. A Thermo Fisher Nicolet iS10 spectrometer (Waltham, MA, United States) was used to obtain the attenuated total reflectance (ATR) IR spectra in the 400–4000 cm^{-1} range. Nitrogen adsorption–desorption isotherms were performed at 77 K using a Micromeritics Asap 2420 porosimeter (York, PA, United States). The samples were first vacuum-treated at 150 °C for 5 h. Thermogravimetric analysis (TGA) was performed using a TA Instrument Q5000IR (New Castle, DE, Germany). TGA analysis was performed under air flow (25 $mL min^{-1}$) up to 650 °C, with a dynamic ramping rate depending on the weight loss.

2.3. Adsorption Experiments

The material (0.4 $g L^{-1}$) and 50 mL of MO aqueous solution of the desired concentration (40–300 $mg L^{-1}$) were placed in an Erlenmeyer flask. The pH of the suspension was adjusted to 5, a typical pH value used to estimate the adsorption efficiency of adsorbents against MO removal. Milli-Q water was used for all experiments. Adsorption experiments were performed in a temperature-controlled incubator. The temperature was set to 25 °C and controlled throughout the adsorption process. The suspensions were under dark conditions throughout the whole experiment. Quantification of the adsorbed MO was performed by recording the UV–Vis spectra using a Varian Cary 100 Scan spectrophotometer. Aliquots of 1.5 mL were periodically taken, and the adsorbent was removed via filtration using a 0.45 μm PTFE Millipore disc. Quantification was based on a comparison to standards. The adsorption capacity was estimated according to following equation:

$$q_e = \frac{(C_0 - C_e) \times V}{m} \quad (1)$$

where q_e ($mg g^{-1}$) is the adsorbed amount at equilibrium; C_0 and C_e ($mg L^{-1}$) are the initial dye concentration and the dye concentration at equilibrium, respectively; V is the volume of the mixture (mL); and m is the mass of the material (mg). The removal efficiency was calculated based on the following equation:

$$R = \frac{(C_0 - C_e) \times 100}{C_0} \quad (2)$$

2.4. Theoretical Simulations

The adsorption data at equilibrium were fitted with a Langmuir-type isotherm [39]:

$$q_e = \frac{q_{\max} \cdot C_e \cdot K_L}{1 + K_L \cdot C_e} \quad (3)$$

where q_e represents the equilibrium dye concentration onto the adsorbents (mg g^{-1}), C_e is the dye concentration in the solution at equilibrium (mg L^{-1}), q_{\max} is the adsorbents' monolayer adsorption capacity (mg L^{-1}), and K_L is the Langmuir adsorption constant (L mg^{-1}). The corresponding linear form of Equation (3) is:

$$\frac{q_e}{C_e} = \frac{1}{q_{\max} \cdot K_L} + \frac{C_e}{q_{\max}} \quad (4)$$

Based on Equation (4), the linear regression between $\frac{q_e}{C_e}$ and C_e was analyzed, and the variables q_{\max} and K_L were estimated.

The pseudo-first- and pseudo-second-order rate-laws were used to fit the kinetic data [34,37]:

$$\frac{dq_t}{dt} = k_1 \cdot (q_e - q_t) \quad (5)$$

$$\frac{dq_t}{dt} = k_2 \cdot (q_e - q_t)^2 \quad (6)$$

The corresponding linear forms of Equations (5) and (6) are:

$$\ln(q_e - q_t) = \ln q_e - k_1 \cdot t \quad (7)$$

$$\frac{1}{q_t} = \frac{1}{k_2 \cdot q_e^2} + \frac{t}{q_e} \quad (8)$$

where q_t is the amount of dye adsorbed onto adsorbents (mg g^{-1}); t is time (min); and k_1 (min^{-1}) and k_2 ($\text{g mg}^{-1} \text{min}^{-1}$) are the first- and second-order adsorption rate coefficients of substance onto adsorbents, respectively. Based on Equations (7) and (8), the linear regression between $\ln(q_e - q_t)$ and $\frac{1}{q_t}$ and t was analyzed, and the variables q_e and K_1 and K_2 were estimated, separately.

The comparison of the theoretical simulations with the experimental data was conducted using the Nash and Sutcliffe efficiency index (E) [40]:

$$E = 1 - \frac{\sum_{i=1}^n (Y_i - S_i)^2}{\sum_{i=1}^n (Y_i - \bar{Y})^2} \quad (9)$$

where n is the number of samples; \bar{Y} is the average of the measured values; and S_i and Y_i are the simulated values by the model and measured data, respectively.

2.5. Recycling Experiments

After the first use, Pal/UiO-66 was collected, redispersed in water, sonicated for 10 min, and thoroughly washed via centrifugation. This process was repeated three times followed by the same procedure once using ethanol. Finally, the solvent was exchanged with acetone over a period of four days and dried overnight at 100 °C. Pal/UiO-66 was reused for adsorption of a 50 mL solution with 60 mg L^{-1} MO. The amount absorbed was calculated via UV-Vis spectroscopy following the same protocol as above.

3. Results and Discussion

3.1. Materials Characterization

Quantification of the clay content in the composite was performed by means of thermogravimetric analysis (TGA). Figure 1 presents the TGA profiles of the pure UiO-66

and Pal as well as that of the Pal/UiO-66 composite. In the Pal sample, there was a smooth drop of the mass until 500 °C, consistent with previous reports [41–43]. The mass loss in the region 80–300 °C was ascribed to surface adsorbed water and to loosely bonded zeolitic water. The mass loss at $T > 300$ °C was attributed to a residual fraction of structural OH_2 . Dehydroxylation is expected at higher temperatures than those applied [41]. Concerning the UiO-66 and the Pal/UiO-66, they both presented similar profiles. A small weight loss was observed in the temperature range 50–400 °C. This was attributed to the removal of guest molecules. The drop of the mass was higher in the Pal/UiO-66 composite in this region probably due to the presence of the clay mineral. In the materials containing the MOF structure, the second mass loss beyond 400 °C was attributed to the oxidation of the framework. This occurred at the same temperature range for both materials. This observation suggests that the thermal stability of UiO-66 is not influenced by the presence of Pal. The final mass of the material at 580 °C was used to quantify the MOF loading. The extracted clay content was ~9 wt.% in the Pal/UiO-66 composite.

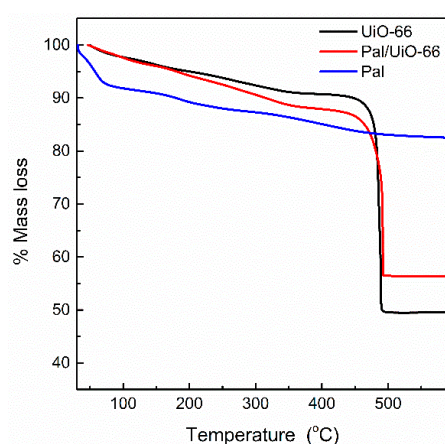


Figure 1. Thermogravimetric analysis (TGA) profiles of the pure UiO-66 and the composite containing palygorskite (Pal).

The structural information of the prepared materials was obtained by performing X-ray diffraction (XRD) analysis. The XRD patterns are given in Figure 2. UiO-66 displayed a diffraction pattern typical for this particular MOF [31,35]. The Pal/UiO-66 composite presented an identical diffraction pattern (Figure 2a). These data indicate that the preparation process adopted for the development of the composite did not affect the formation of UiO-66. No diffraction peaks related with Pal were detected in the composite. The inability to detect any diffraction peaks related with Pal probably occurred due to two reasons. First, the amount of Pal in the composite was low, as evidenced by the results of thermogravimetric analysis. Second, UiO-66 had an intense diffraction peak in the region where the main diffraction peak of Pal was expected (ca. 8.5°) [15,25]. Palygorskite has good acid resistant properties [44]; however, in order to verify its stability, Pal was treated under the synthesis conditions applied in the absence of the MOF precursors. The XRD patterns of the treated Pal were similar to those of the parent sample (Figure 2b). This observation suggests that Pal is stable under the conditions adopted for UiO-66 synthesis and that the inability to detect any diffraction peaks assigned to Pal in the composite sample probably originates from the low Pal content.

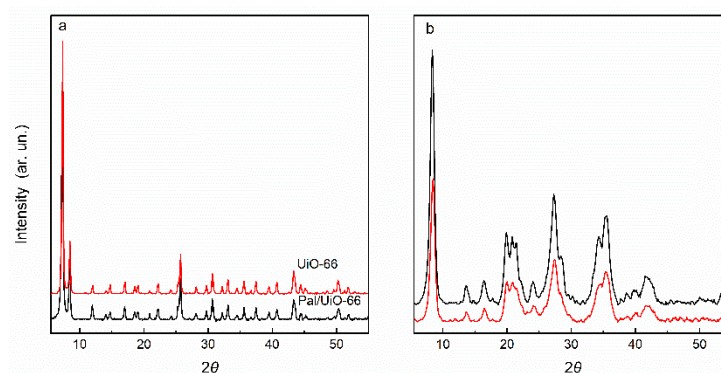


Figure 2. X-ray diffraction (XRD) patterns of the prepared materials, UiO-66, and the Pal/UiO-66 composite (a) and the Pal sample before and after being treated under the synthesis conditions (b).

The materials were further studied using attenuated total reflection Fourier transform infrared (ATR-FTIR) spectroscopy (Figure 3). All characteristic vibrational modes of UiO-66 were detected [45–47]. The two intense peaks centered at 1392 and 1582 cm^{-1} were assigned to the asymmetric and symmetric stretch vibrations in the carboxylate group of the organic ligand. The sharp peak at ca. 1510 cm^{-1} was assigned to the vibration of the C=C in the benzene ring. The peaks in the region 667–745 cm^{-1} originated from the O–H and C–H vibrations modes of the organic linker. The vibration mode at 555 cm^{-1} was attributed to the Zr-(OC) asymmetric stretch. These observations agree with those in previous reports [45–47]. The Pal/UiO-66 presents a similar ATR spectrum to that of pure UiO-66. These results further suggest that the presence of Pal did not affect the synthesis of the MOF. The vibrational mode of the pure UiO-66 centered at 1582 cm^{-1} shifted to a higher wavenumber (1588 cm^{-1}). This shift may suggest an interaction of the organic part of the MOF with the clay mineral through the carboxylate groups. In addition to the peaks related with UiO-66, the Pal/UiO-66 composite presented a broad peak in the range 970–1060 cm^{-1} that was not seen in the pure UiO-66 (indicated with the arrow in the inset in Figure 2). This was attributed to Pal and corresponded to the Si-O-Mg asymmetric stretching vibration [26,44,47]. Peaks in the region 1650 cm^{-1} were also detected in Pal/UiO-66 material, attributed to the OH bending vibration of adsorbed water on the clay structure [44]. Overall, the results of ATR verified the presence of both phases in the composite and suggested an interaction between them.

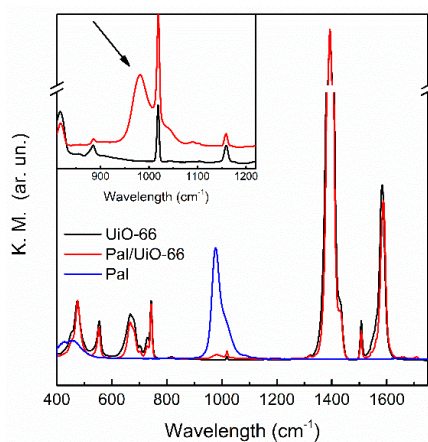


Figure 3. Attenuated total reflectance Fourier infrared spectroscopy (ATR-FTIR) spectra of Pal, UiO-66, and composite containing palygorskite (Pal).

Because specific surface area plays a vital role in adsorption reactions, the Brunauer–Emmett–Teller (BET) surface area was determined for the prepared materials by N_2 adsorption–desorption isotherms at 77 K. The data are given in Figure 4. The pure UiO-66

had a BET specific surface area (SSA) of $929.0 \text{ m}^2 \text{ g}^{-1}$, in accordance with the literature [35]. Pal had a low SSA ($174.3 \text{ m}^2 \text{ g}^{-1}$). The introduction of palygorskite in the composite resulted in an increased BET SSA, $1086.5 \text{ m}^2 \text{ g}^{-1}$. An increase in the SSA of MOF-based composites compared with the bare MOF structure has been previously seen [48,49]. Herein, this was most likely linked with the formation of porosity at the interface formed between the two parts in the composite, as shown by Petit and Bandosz [48]. An interface between the two parts probably formed due to the in situ strategy applied for the development of the Pal/UiO-66 composite, as also suggested by the findings of ATR spectroscopy. The increased surface area of the composite in comparison with that of the pure MOF structure is expected to affect the adsorption properties.

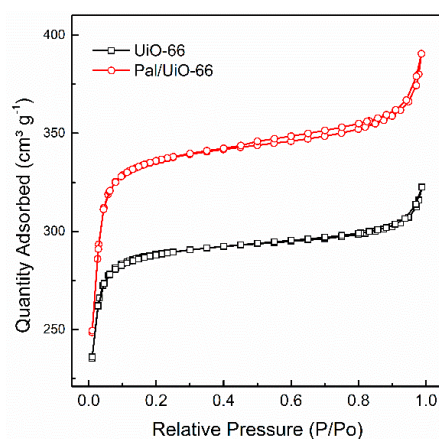


Figure 4. N_2 adsorption–desorption isotherms for pure UiO-66 and Pal/UiO-66 composite.

3.2. Dye Adsorption Evaluation

The effect of contact time on the adsorption over the pure UiO-66 and Pal materials as well as the Pal/UiO-66 composite was first evaluated. The data are given in Figure 5a. Pure Pal had low adsorption efficiency over MO. This was expected because under the conditions of the adsorption experiments, both Pal and MO were negatively charged [15,23,50], resulting in an electrostatic repulsion force generated between the adsorbent and MO. On the contrary, both pure UiO-66 and Pal/UiO-66 presented significant adsorption efficiency against MO removal (Figure 5a). Considering that the adsorption efficiency of Pal was very low compared with that of pure UiO-66, the Pal content in the composite was kept low during the synthesis process. Taking into account the adsorption kinetics using UiO-66 and Pal/UiO-66 in Figure 5a, specifically the fast adsorption process that was completed within 5 min and the high removal efficiencies, both UiO-66 and Pal/UiO-66 could effectively and quickly remove MO from water. We also highlight that the high sorption rates that led to the almost immediate achievement of equilibrium using the materials containing UiO-66 in this study (i.e., ~5 min) are not usual for this specific MOF family, which is used as adsorbents for similar substrates [35,39].

The adsorption kinetic curves for pure UiO-66 and Pal/UiO-66 composite as a function of time, fitted using a pseudo-first-order and pseudo-second-order kinetic model, are shown in Figure 5b,c, respectively. As evidenced, the pseudo-second-order kinetic model better described the adsorption data for both materials. The correlation coefficient R^2 for the pseudo-second-order kinetic model ($R^2 > 0.999$) was acceptable for both materials. In addition, the calculated adsorption at equilibrium ($q_{e,cal}$) using the pseudo-second-order kinetic model matched the experimentally obtained values ($q_{e,exp}$) for both materials. The correlation coefficient R^2 for the pseudo-first-order model was not sufficient, and the model did not reproduce the experimental $q_{e,exp}$.

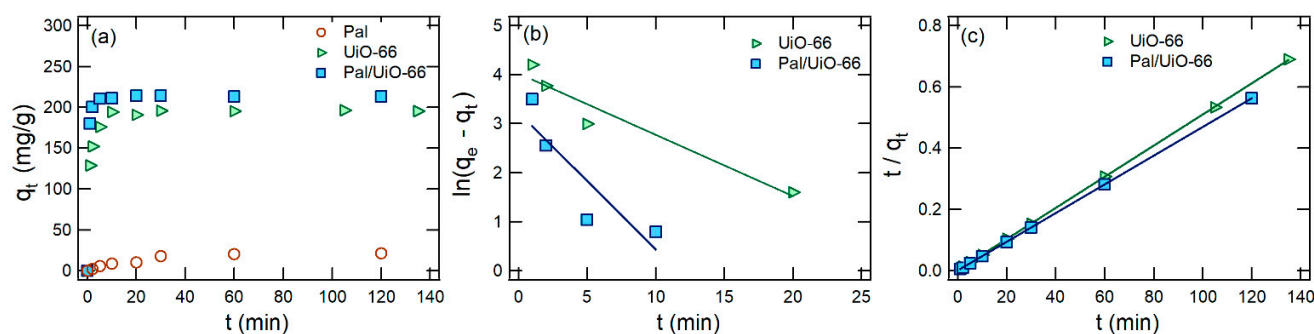


Figure 5. Time dependence of MO adsorption on the pure UiO-66 and Pal samples as well as the Pal/UiO-66 composite material (a). Plots of pseudo-first- (b) and pseudo-second-order rate-law (c) for MO adsorption on pure the UiO-66 and Pal/UiO-66 composite. Experimental conditions: 90 mg L^{-1} initial MO concentration, 0.4 g L^{-1} of the adsorbent, $\text{pH} = 5$, volume 50 mL , and $T = 25 \text{ }^\circ\text{C}$.

The adsorption isotherms of MO over UiO-66 and Pal/UiO-66 are given in Figure 6a. The Pal/UiO-66 composite presented superior adsorption capacity compared with pure UiO-66. The removal efficiency of Pal/UiO-66 against MO was 94.7%, while pure UiO-66 removed only 86.7% at an initial MO concentration 90 mg L^{-1} . A similar increase in the removal efficiency was also observed at higher initial MO concentrations, i.e., 67.8% and 57.8% for Pal/UiO-66 and pure UiO-66, respectively, using 180 mg L^{-1} initial MO concentration. An impressive maximum equilibrium adsorption capacity ($q_{\text{max,exp}}$) was obtained for the composite material (ca. 340 mg g^{-1}), which is among the highest reported in the literature using UiO-66-based materials [35,39,51,52]. This was more important considering that the MOF structure accounted for only 90 wt.% of the composite material. The maximum equilibrium adsorption capacity was further increased to 378 mg g^{-1} considering only the mass of the UiO-66 in the composite. This corresponded to a 34.5% increase in q_{max} compared with that of pure UiO-66.

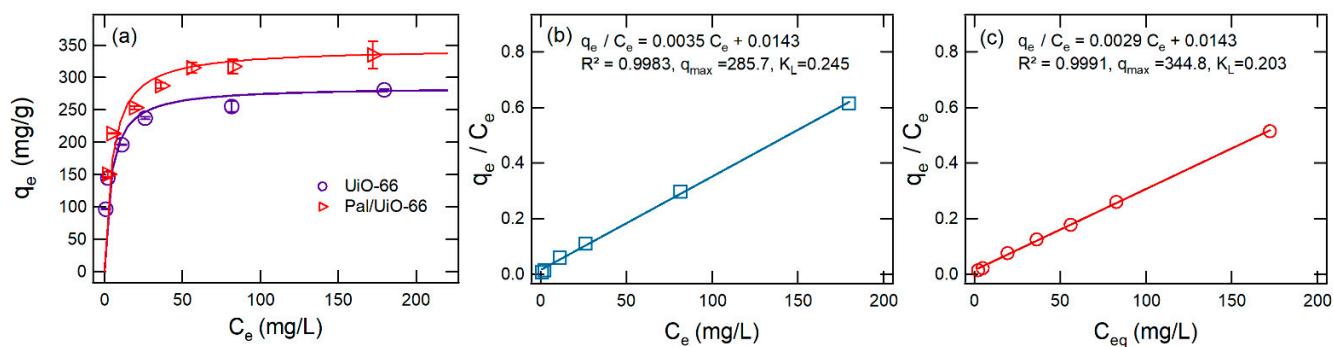


Figure 6. Adsorption isotherms using different MO initial concentration on the pure UiO-66 and composite material (a). Isotherms based on the Langmuir model for pure UiO-66 (b) and Pal/UiO-66 (c) and the corresponding isotherms parameters. Experimental conditions: initial MO concentration $40\text{--}300 \text{ mg L}^{-1}$, 0.4 g L^{-1} of the adsorbent, $\text{pH} = 5$, volume 50 mL , and $T = 25 \text{ }^\circ\text{C}$.

For further insights regarding the adsorption behavior, the Langmuir model was used to simulate the isotherm data (Figure 6b,c) [35,39]. As evidenced by the R^2 values (0.9983 and 0.9991 for pure UiO-66 and composite material, respectively), the Langmuir model described the isotherm data well. In addition, the calculated maximum equilibrium adsorption capacity ($q_{\text{max,cal}} = 285.7$ and 344.8 mg g^{-1} for UiO-66 and composite material, respectively) matched the experimental values in both cases ($q_{\text{max,exp}} = 281$ and 340 mg g^{-1} for UiO-66 and Pal/UiO-66, respectively). The isotherms parameters are also given in Figure 6b,c.

Stability is a critical parameter and a prerequisite for practical applications. UiO-66 is highly stable adsorbent for dye adsorption from aqueous media including MO [35]. The

stability of the prepared composite under working conditions was tested by contacting recycling experiments. As evidenced in Figure 7, Pal/UiO-66 retained more than 91% of its adsorption efficiency after five consecutive uses compared with the fresh material. These results indicate its high potential as a reusable adsorption material.

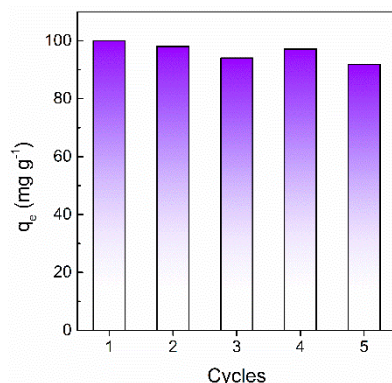


Figure 7. Removal efficiency of Pal/UiO-66 over five consecutive cycles. Experimental conditions: 60 mg L⁻¹ initial MO concentration, 0.4 g L⁻¹ of the adsorbent, pH = 5, volume 50 mL, and T = 25 °C.

4. Conclusions

An easy open vessel thermal process was developed for the efficient in situ coupling of UiO-66 with palygorskite clay mineral, allowing the development of a composite. Both structures were unaltered in the composite. Palygorskite presented low adsorption capacity against MO. On the contrary, both UiO-66 and Pal/UiO-66 presented excellent adsorption capacity. Comparing the materials containing UiO-66, the composite presented 21% enhanced maximum equilibrium adsorption capacity compared with that of the pure UiO-66. This enhancement was further improved to 34.5% considering the actual content of the MOF structure. Pal/UiO-66 was also proven to be highly recyclable, losing less than 9% of its adsorption capacity after five recycles. The present study highlights the importance of coupling MOF structures with low-cost clay minerals for the development of advanced adsorbents.

Author Contributions: Conceptualization, I.A.V. and K.C.C.; methodology, I.A.V. and K.C.C.; validation, I.A.V., K.C.C. and D.P.; formal analysis, I.A.V.; investigation, I.A.V., T.I., M.A. and A.P.; Resources, K.C.C. and D.P.; data curation, I.A.V., T.I., M.A., D.P. and K.C.C.; writing—original draft preparation, I.A.V. and K.C.C.; writing—review and editing, I.A.V., D.P. and K.C.C.; visualization, I.A.V. and M.A.; supervision, I.A.V. and K.C.C.; project administration, I.A.V. and K.C.C.; funding acquisition, K.C.C. All authors have read and agreed to the published version of the manuscript.

Funding: This work benefited from state aid managed by the French National Research Agency (ANR) under the Investments for the Future (program “Make Our Planet Great Again”) with reference ANR-18-MOPGA-0014. The research was partially funded by Democritus University of Thrace (project 82268).

Institutional Review Board Statement: Not applicable.

Informed Consent Statement: Not applicable.

Conflicts of Interest: The authors declare no conflict of interest.

References

1. Saravanan, A.; Kumar, P.S.; Yaashikaa, P.R.; Karishma, S.; Jeevanantham, S.; Swetha, S. Mixed Biosorbent of Agro Waste and Bacterial Biomass for the Separation of Pb(II) Ions from Water System. *Chemosphere* **2021**, *277*, 130236. [[CrossRef](#)] [[PubMed](#)]
2. Jiang, D.; Chen, M.; Wang, H.; Zeng, G.; Huang, D.; Cheng, M.; Liu, Y.; Xue, W.; Wang, Z. The Application of Different Typological and Structural MOFs-Based Materials for the Dyes Adsorption. *Coord. Chem. Rev.* **2019**, *380*, 471–483. [[CrossRef](#)]
3. Uddin, M.J.; Ampiauw, R.E.; Lee, W. Adsorptive Removal of Dyes from Wastewater Using a Metal-Organic Framework: A Review. *Chemosphere* **2021**, *284*, 131314. [[CrossRef](#)] [[PubMed](#)]

4. Murugesan, A.; Loganathan, M.; Senthil Kumar, P.; Vo, D.-V.N. Cobalt and Nickel Oxides Supported Activated Carbon as an Effective Photocatalysts for the Degradation Methylene Blue Dye from Aquatic Environment. *Sustain. Chem. Pharm.* **2021**, *21*, 100406. [[CrossRef](#)]
5. Renita, A.A.; Vardhan, K.H.; Kumar, P.S.; Nguéagni, P.T.; Abilarasu, A.; Nath, S.; Kumari, P.; Saravanan, R. Effective Removal of Malachite Green Dye from Aqueous Solution in Hybrid System Utilizing Agricultural Waste as Particle Electrodes. *Chemosphere* **2021**, *273*, 129634. [[CrossRef](#)]
6. Liang, J.; Ning, X.; Sun, J.; Song, J.; Lu, J.; Cai, H.; Hong, Y. Toxicity Evaluation of Textile Dyeing Effluent and Its Possible Relationship with Chemical Oxygen Demand. *Ecotoxicol. Environ. Saf.* **2018**, *166*, 56–62. [[CrossRef](#)]
7. Katheresan, V.; Kannedo, J.; Lau, S.Y. Efficiency of Various Recent Wastewater Dye Removal Methods: A Review. *J. Environ. Chem. Eng.* **2018**, *6*, 4676–4697. [[CrossRef](#)]
8. Bhatia, D.; Sharma, N.R.; Singh, J.; Kanwar, R.S. Biological Methods for Textile Dye Removal from Wastewater: A Review. *Crit. Rev. Environ. Sci. Technol.* **2017**, *47*, 1836–1876. [[CrossRef](#)]
9. Wong, S.; Ghafar, N.A.; Ngadi, N.; Razmi, F.A.; Inuwa, I.M.; Mat, R.; Amin, N.A.S. Effective Removal of Anionic Textile Dyes Using Adsorbent Synthesized from Coffee Waste. *Sci. Rep.* **2020**, *10*, 2928. [[CrossRef](#)]
10. Robinson, T.; McMullan, G.; Marchant, R.; Nigam, P. Remediation of Dyes in Textile Effluent: A Critical Review on Current Treatment Technologies with a Proposed Alternative. *Bioresour. Technol.* **2001**, *77*, 247–255. [[CrossRef](#)]
11. Au, V.K.-M. Recent Advances in the Use of Metal-Organic Frameworks for Dye Adsorption. *Front. Chem.* **2020**, *8*, 708. [[CrossRef](#)] [[PubMed](#)]
12. Abhinaya, M.; Parthiban, R.; Kumar, P.S.; Vo, D.-V.N. A Review on Cleaner Strategies for Extraction of Chitosan and Its Application in Toxic Pollutant Removal. *Environ. Res.* **2021**, *196*, 110996. [[CrossRef](#)] [[PubMed](#)]
13. Sharma, G.; AlGarni, T.S.; Kumar, P.S.; Bhogal, S.; Kumar, A.; Sharma, S.; Naushad, M.; AlOthman, Z.A.; Stadler, F.J. Utilization of Ag₂O–Al₂O₃–ZrO₂ Decorated onto RGO as Adsorbent for the Removal of Congo Red from Aqueous Solution. *Environ. Res.* **2021**, *197*, 111179. [[CrossRef](#)] [[PubMed](#)]
14. Ullah, S.; Al-Sehemi, A.G.; Mubashir, M.; Mukhtar, A.; Saqib, S.; Bustam, M.A.; Cheng, C.K.; Ibrahim, M.; Show, P.L. Adsorption Behavior of Mercury over Hydrated Lime: Experimental Investigation and Adsorption Process Characteristic Study. *Chemosphere* **2021**, *271*, 129504. [[CrossRef](#)]
15. Yang, R.; Li, D.; Li, A.; Yang, H. Adsorption Properties and Mechanisms of Palygorskite for Removal of Various Ionic Dyes from Water. *Appl. Clay Sci.* **2018**, *151*, 20–28. [[CrossRef](#)]
16. Salleh, M.A.M.; Mahmoud, D.K.; Karim, W.A.W.A.; Idris, A. Cationic and Anionic Dye Adsorption by Agricultural Solid Wastes: A Comprehensive Review. *Desalination* **2011**, *280*, 1–13. [[CrossRef](#)]
17. Cheung, W.H.; Szeto, Y.S.; McKay, G. Enhancing the Adsorption Capacities of Acid Dyes by Chitosan Nano Particles. *Bioresour. Technol.* **2009**, *100*, 1143–1148. [[CrossRef](#)]
18. Belaid, K.D.; Kacha, S.; Kameche, M.; Derriche, Z. Adsorption Kinetics of Some Textile Dyes onto Granular Activated Carbon. *J. Environ. Chem. Eng.* **2013**, *1*, 496–503. [[CrossRef](#)]
19. Li, C.-P.; Zhou, H.; Chen, J.; Wang, J.-J.; Du, M.; Zhou, W. A Highly Efficient Coordination Polymer for Selective Trapping and Sensing of Perrhenate/Perthentate. *ACS Appl. Mater. Interfaces* **2020**, *12*, 15246–15254. [[CrossRef](#)]
20. Abidi, N.; Errais, E.; Duplay, J.; Berez, A.; Jrad, A.; Schäfer, G.; Ghazi, M.; Semhi, K.; Trabelsi-Ayadi, M. Treatment of Dye-Containing Effluent by Natural Clay. *J. Clean. Prod.* **2015**, *86*, 432–440. [[CrossRef](#)]
21. Lagaly, G. *Colloid Clay Science. Developments in Clay Science*; Bergaya, F., Theng, B.K.G., Lagaly, G., Eds.; Elsevier Science: Amsterdam, The Netherlands, 2006; Volume 1, pp. 141–245. ISBN 978-0-08-044183-2.
22. Moreira, M.A.; Ciuffi, K.J.; Rives, V.; Vicente, M.A.; Trujillano, R.; Gil, A.; Korili, S.A.; de Faria, E.H. Effect of Chemical Modification of Palygorskite and Sepiolite by 3-Aminopropyltriethoxysilane on Adsorption of Cationic and Anionic Dyes. *Appl. Clay Sci.* **2017**, *135*, 394–404. [[CrossRef](#)]
23. Middea, A.; Spinelli, L.S.; Souza, F.G., Jr.; Neumann, R.; Fernandes, T.L.A.P.; Gomes, O.d.F.M. Preparation and Characterization of an Organo-Palygorskite-Fe₃O₄ Nanomaterial for Removal of Anionic Dyes from Wastewater. *Appl. Clay Sci.* **2017**, *139*, 45–53. [[CrossRef](#)]
24. García-Romero, E.; Suárez, M. On the Chemical Composition of Sepiolite and Palygorskite. *Clays Clay Miner.* **2010**, *58*, 1–20. [[CrossRef](#)]
25. Papoulis, D.; Komarneni, S.; Panagiotaras, D.; Nikolopoulou, A.; Christoforidis, K.C.; Fernández-García, M.; Li, H.; Shu, Y.; Sato, T. Palygorskite-TiO₂ Nanocomposites: Part 2. Photocatalytic Activities in Decomposing Air and Organic Pollutants. *Appl. Clay Sci.* **2013**, *83–84*, 198–202. [[CrossRef](#)]
26. Papoulis, D.; Komarneni, S.; Panagiotaras, D.; Stathatos, E.; Christoforidis, K.C.; Fernández-García, M.; Li, H.; Shu, Y.; Sato, T.; Katsuki, H. Three-Phase Nanocomposites of Two Nanoclays and TiO₂: Synthesis, Characterization and Photocatalytic Activities. *Appl. Catal. B Environ.* **2014**, *147*, 526–533. [[CrossRef](#)]
27. Papoulis, D.; Panagiotaras, D.; Tsigrou, P.; Christoforidis, K.C.; Petit, C.; Apostolopoulou, A.; Stathatos, E.; Komarneni, S.; Koukouvelas, I. Halloysite and Sepiolite-TiO₂ nanocomposites: Synthesis Characterization and Photocatalytic Activity in Three Aquatic Wastes. *Mater. Sci. Semicond. Process.* **2018**, *85*, 1–8. [[CrossRef](#)]
28. Chen, H.; Zhong, A.; Wu, J.; Zhao, J.; Yan, H. Adsorption Behaviors and Mechanisms of Methyl Orange on Heat-Treated Palygorskite Clays. *Ind. Eng. Chem. Res.* **2012**, *51*, 14026–14036. [[CrossRef](#)]

29. Zhao, G.; Shi, L.; Feng, X.; Yu, W.; Zhang, D.; Fu, J. Palygorskite-Cerium Oxide Filled Rubber Nanocomposites. *Appl. Clay Sci.* **2012**, *67–68*, 44–49. [[CrossRef](#)]
30. Crake, A.; Christoforidis, K.C.; Gregg, A.; Moss, B.; Kafizas, A.; Petit, C. The Effect of Materials Architecture in TiO₂/MOF Composites on CO₂ Photoreduction and Charge Transfer. *Small* **2019**, *15*, e1805473. [[CrossRef](#)]
31. Crake, A.; Christoforidis, K.C.; Kafizas, A.; Zafeiratos, S.; Petit, C. CO₂ Capture and Photocatalytic Reduction Using Bifunctional TiO₂/MOF Nanocomposites under UV-Vis Irradiation. *Appl. Catal. B Environ.* **2017**, *210*, 131–140. [[CrossRef](#)]
32. Zhang, Y.; Jiang, Z.; Song, J.; Song, J.; Pan, F.; Zhang, P.; Cao, X. Elevated Pervaporative Desulfurization Performance of Pebax-Ag⁺@MOFs Hybrid Membranes by Integrating Multiple Transport Mechanisms. *Ind. Eng. Chem. Res.* **2019**, *58*, 16911–16921. [[CrossRef](#)]
33. Haque, E.; Lee, J.E.; Jang, I.T.; Hwang, Y.K.; Chang, J.-S.; Jegal, J.; Jung, S.H. Adsorptive Removal of Methyl Orange from Aqueous Solution with Metal-Organic Frameworks, Porous Chromium-Benzenedicarboxylates. *J. Hazard. Mater.* **2010**, *181*, 535–542. [[CrossRef](#)] [[PubMed](#)]
34. Winarta, J.; Shan, B.; McIntyre, S.M.; Ye, L.; Wang, C.; Liu, J.; Mu, B. A Decade of UiO-66 Research: A Historic Review of Dynamic Structure, Synthesis Mechanisms, and Characterization Techniques of an Archetypal Metal-Organic Framework. *Cryst. Growth Des.* **2020**, *20*, 1347–1362. [[CrossRef](#)]
35. Yang, J.-M. A Facile Approach to Fabricate an Immobilized-Phosphate Zirconium-Based Metal-Organic Framework Composite (UiO-66-P) and Its Activity in the Adsorption and Separation of Organic Dyes. *J. Colloid Interface Sci.* **2017**, *505*, 178–185. [[CrossRef](#)] [[PubMed](#)]
36. Chen, Q.; He, Q.; Lv, M.; Xu, Y.; Yang, H.; Liu, X.; Wei, F. Selective Adsorption of Cationic Dyes by UiO-66-NH₂. *Appl. Surf. Sci.* **2015**, *327*, 77–85. [[CrossRef](#)]
37. Shahriyari Far, H.; Hasanzadeh, M.; Najafi, M.; Rahimi, R. In-Situ Self-Assembly of Mono- and Bi-Metal Organic Frameworks onto Clay Mineral for Highly Efficient Adsorption of Pollutants from Wastewater. *Chem. Phys. Lett.* **2022**, *799*, 139626. [[CrossRef](#)]
38. Zhao, Y.; Zhang, Q.; Li, Y.; Zhang, R.; Lu, G. Large-Scale Synthesis of Monodisperse UiO-66 Crystals with Tunable Sizes and Missing Linker Defects via Acid/Base Co-Modulation. *ACS Appl. Mater. Interfaces* **2017**, *9*, 15079–15085. [[CrossRef](#)]
39. Lv, S.-W.; Liu, J.-M.; Ma, H.; Wang, Z.-H.; Li, C.-Y.; Zhao, N.; Wang, S. Simultaneous Adsorption of Methyl Orange and Methylene Blue from Aqueous Solution Using Amino Functionalized Zr-Based MOFs. *Microporous Mesoporous Mater.* **2019**, *282*, 179–187. [[CrossRef](#)]
40. Nash, J.E.; Sutcliffe, J.V. River Flow Forecasting through Conceptual Models Part I—A Discussion of Principles. *J. Hydrol.* **1970**, *10*, 282–290. [[CrossRef](#)]
41. Giustetto, R.; Compagnoni, R. An Unusual Occurrence of Palygorskite from Montestrutto, Sesia-Lanzo Zone, Internal Western Alps (Italy). *Clay Miner.* **2011**, *46*, 371–385. [[CrossRef](#)]
42. Giustetto, R.; Chiari, G. Crystal Structure Refinement of Palygorskite from Neutron Powder Diffraction. *Eur. J. Mineral.* **2004**, *16*, 521–532. [[CrossRef](#)]
43. Giustetto, R.; Seenivasan, K.; Pellerej, D.; Ricchiardi, G.; Bordiga, S. Spectroscopic Characterization and Photo/Thermal Resistance of a Hybrid Palygorskite/Methyl Red Mayan Pigment. *Microporous Mesoporous Mater.* **2012**, *155*, 167–176. [[CrossRef](#)]
44. Zhu, J.; Zhang, P.; Wang, Y.; Wen, K.; Su, X.; Zhu, R.; He, H.; Xi, Y. Effect of Acid Activation of Palygorskite on Their Toluene Adsorption Behaviors. *Appl. Clay Sci.* **2018**, *159*, 60–67. [[CrossRef](#)]
45. Tang, J.; Dong, W.; Wang, G.; Yao, Y.; Cai, L.; Liu, Y.; Zhao, X.; Xu, J.; Tan, L. Efficient Molybdenum(VI) Modified Zr-MOF Catalysts for Epoxidation of Olefins. *RSC Adv.* **2014**, *4*, 42977–42982. [[CrossRef](#)]
46. Zhang, Q.; Yang, T.; Liu, X.; Yue, C.; Ao, L.; Deng, T.; Zhang, Y. Heteropoly Acid-Encapsulated Metal-Organic Framework as a Stable and Highly Efficient Nanocatalyst for Esterification Reaction. *RSC Adv.* **2019**, *9*, 16357–16365. [[CrossRef](#)]
47. Han, Y.; Liu, M.; Li, K.; Zuo, Y.; Wei, Y.; Xu, S.; Zhang, G.; Song, C.; Zhang, Z.; Guo, X. Facile Synthesis of Morphology and Size-Controlled Zirconium Metal-Organic Framework UiO-66: The Role of Hydrofluoric Acid in Crystallization. *CrystEngComm* **2015**, *17*, 6434–6440. [[CrossRef](#)]
48. Petit, C.; Bandoz, T.J. Engineering the Surface of a New Class of Adsorbents: Metal-Organic Framework/Graphite Oxide Composites. *J. Colloid Interface Sci.* **2015**, *447*, 139–151. [[CrossRef](#)]
49. Muschi, M.; Devautour-Vinot, S.; Aureau, D.; Heymans, N.; Sene, S.; Emmerich, R.; Ploumistos, A.; Geneste, A.; Steunou, N.; Patriarche, G.; et al. Metal-Organic Framework/Graphene Oxide Composites for CO₂ Capture by Microwave Swing Adsorption. *J. Mater. Chem. A* **2021**, *9*, 13135–13142. [[CrossRef](#)]
50. Middea, A.; Fernandes, T.L.A.P.; Neumann, R.; Gomes, F.M.O.; Spinelli, L.S. Evaluation of Fe(III) Adsorption onto Palygorskite Surfaces. *Appl. Surf. Sci.* **2013**, *282*, 253–258. [[CrossRef](#)]
51. Beydaghdari, M.; Hooriabad Saboor, F.; Babapoor, A.; Karve, V.V.; Asgari, M. Recent Advances in MOF-Based Adsorbents for Dye Removal from the Aquatic Environment. *Energies* **2022**, *15*, 2023. [[CrossRef](#)]
52. Nanthamathee, C.; Chantarangkul, C.; Jakkrawhad, C.; Payaka, A.; Dechatiwongse, P. Fine-Tuning the Dye Adsorption Capacity of UiO-66 by a Mixed-Ligand Approach. *Heliyon* **2022**, *8*, e08961. [[CrossRef](#)] [[PubMed](#)]